JREE: Vol. 7, No. 3, (Summer 2020) 56-66

Journal of Renewable Energy and Environment

Research Article

Journal Homepage: www.jree.ir

Quantification of Thermal Energy Performance Improvement for Building Integrated Photovoltaic Double-Skin Façade Using Analytical Method

Mahdi Shakouri[a], Alireza Noorpoor[a*], Hossein Ghadamian[b]

[a] *Department of Environmental Engineering, School of Environment, College of Engineering, University of Tehran, P. O. Box: 11155-4563, Tehran, Iran.*
[b] *Department of Energy, Materials and Energy Research Center (MERC), MeshkinDasht, Alborz, Iran.*

PAPER INFO

Paper history:
Received 25 April 2020
Accepted in revised form 13 July 2020

Keywords:
Analytical Method
Building Integrated Photovoltaic Thermal
Double Skin Façade
Energy Saving
Thermal Performance

ABSTRACT

This study presents an analytical method for quantifying the improvement of thermal energy performance of a building integrated photovoltaic double-skin façade. The system was suggested as a retrofit measure for an existing building in Tehran. The effect of thermal performance was analyzed through computer-assisted developed codes using Engineering Equation Solver (EES) software. Three scenarios were defined and for each scenario, temperature and velocity profiles were provided through continuity, momentum, and energy equations. Given that the monocrystalline photovoltaic modules and the double-glazed windows are quite common in the current condition in Tehran, the authors considered them for analysis. A comparison of results is valuable for those cases that intend to select either glass or photovoltaic as the outer façade. The quantitative results illustrate that the proposed system would reduce the cooling demand in the summer case by 18.5 kilowatts, which is around 8.7 percent of the current cooling load. According to the results of the sensitivity analysis, both glass and photovoltaic façades were of greater efficiency in terms of energy saving in the summer. By increasing the ratio between the photovoltaic outer façade to the surface area of the glass section, the amount of energy saving due to the total cooling load reduction will increase. The results of the analysis showed that the application of the suggested system would reduce the thermal load by 2.1 percent in the winter season.

1. INTRODUCTION

New designs of façades should ensure a comfortable indoor climate, soundproof, use of daylighting, and reduced energy demand. Nowadays, Double-Skin Façades (DSFs) have become an increasing and important architectural element in buildings in combination with Photovoltaic (PV) panels.

Considering the need to use more renewable energy, investigation of Building Integrated Photovoltaic (BIPV) systems to improve their performance is of great importance [1]. Solar façades are designed to specifically reject or absorb and reutilize solar heat [2]. Because PV panels are heat sources in BIPV, such systems are often designed with the ability to provide ventilation through the solar chimney principle combined with a DSF design concept.

Thus, the self-ventilating and self-heat dissipation mechanisms of BIPV are realized through natural ventilation and buoyant force [3]. From the efficiency perspective of PV panel, typically 5-25 % of radiated solar energy on the PV panel front surface is transformed into electricity [4] and the remaining is transformed into heat [5].Because the solar cell temperature affects the generation efficiency of a PV module [6], PV modules have evolved with advances in BIPV from the units directly attached to a building envelope to the units detached from it. Therefore, appropriate cooling technologies must be used for enhancing the efficiency of panels. Recently, some researchers have attempted to develop thermal models to estimate the operating temperature of the PV system considering finer details of heat transfer. The methods of energy transfer from the PV module to the surroundings were theoretically modeled [7].

An investigation into the performance of a system that integrates a PV layer into a DSF using a simulated dynamic thermal behavior of the system leads to a reduction in the monthly cooling energy demand between 20-30 %. This result is particularly relevant to hot climates, where cooling loads are seen throughout the year [8]. Zogou and Stapountzis [9] installed a Double-Skin Façade Building Integrated Photovoltaic (DSF-BIPV) system on the south-facing façade of an office building and directed the channel flow heated by the DSF to indoor areas to warm and ventilate rooms. Rabani et al. [10] designed an air outlet in the form of DSF where the indoor air was drawn out of the building through a solar chimney effect and a water spraying system was installed in the air inlet to cool the air drawn from the outdoors. Corbin and Zhai [11] designed a Building Integrated Photovoltaic Thermal (BIPVT) system that was integrated with PV and a solar hot water heater, which increased the efficiency of the solar cell by 5.3 %. Shakouri et al. [12] reviewed the electrical and thermal performance of Photovoltaic Thermal (PVT) systems through optimization using a genetic algorithm in MATLAB software. Shakouri et al. [13] simulated a photovoltaic thermal system and thereafter, evaluated the overall performance of the system through parametric analysis. Pantic et al. [14] analyzed the energy performance of three different types of BIPVT systems. Outdoor air is directed through these systems, and heated air flows over the rock substrate where it is stored, whereas solar energy is stored through the sensible heat capacity of the rock. The energy performance of different types of glazing was compared to determine the best long-term comfort conditions

*Corresponding Author's Email: noorpoor@ut.ac.ir (A. Noorpoor)

in an open-space office with the climatic conditions of Paris, Milan, and Rome [15]. Serra et al. [16] directed air into the air-flow channel of a double-glazed facade through mechanical ventilation. Both clear glass and low emissivity glass were used as the transparent building materials, whereas Venetian blinds and polyvinyl chloride reflecting roller screens were used as the shading louvers. Ghadimi et al. [17] assessed the energy performance of multiple skin façade utilizing experiments and numerical simulations. Fuliotto et al. [18] developed the decoupling method for simulating the thermal properties of a ventilated double-glazed façade with a Venetian blind. Kuznik et al. [19] developed a simulation method using the zonal model approach and radiative/convective heat transfers, and they investigated the effects of airflow rates and blade angles on the heat transfer performance of a ventilated double-glazed façade with a Venetian blind. Mulyadi et al. [20] simulated the thermal performance of a ventilated double-glazed facade with a light-colored horizontal blind that extended over five stories of a building in Indonesia. Hoseinzadeh et al. [21-23] analyzed the energy consumption improvements of a zero-energy building in a humid mountainous area. They reviewed the thermal performance of electrochromic smart windows with nanocomposite structures under different climates in Iran. Thereafter, they have simulated and optimized a solar-assisted heating and cooling system for a house in the Northern part of Iran. Yousef Nezhad and Hoseinzadeh carried out their research on the mathematical modeling and simulation of a solar water heater for an aviculture unit using MATLAB [24]. According to the results, 80 % of the amount of electrical energy was used for air conditioning in the building and energy consumption decreased from 34 to 7 MW. In the case of Return on Investment (RoI), the electricity needs to be generated and the cost can be about $ 15,000 a year [21-24]. Multi-glazed façades can effectively cut off the conductive and convective heat transfer of the solar heat gain and radiative heat transfers are usually blocked through the reflective or absorptive characteristics of the coating material on the glass [16]. Thermal models developed so far require further modification and they could include heat loss from PV panel front and back surfaces into the environment, heat loss due to radiation, variable climatic conditions, and the effect of PV panel inclination angle on heat loss mechanisms [7].

Given that the research team has reviewed the researches done by other researchers, they found no appropriate and thorough analysis of the outer façade with a combined structure of both glass and photovoltaic modules. Thus, authors have focused on this research gap and tried to simulate the outer façade with the above-mentioned structure within the studied case, which is the existing office building in Tehran. The results of this study are interesting for both decision-makers and design engineers as the current cooling load peak in the summer case has become a concern for Iran. This type of suggested energy-saving measure can be considered as one of the proper solutions for the building sector to tackle the issue of cooling load peak in the summer case.

The present study provides one step further in Building Integrated Photovoltaic Thermal Double-Skin Façade (BIPVT-DSF) system and investigates the thermal performance through an analytical solution. The methods of solution applied to the current research and investigation are borrowed from a previous study on DSF [25]. However, this research provides a new approach to BIPVT-DSF as the application of both glass and PV façades has been considered as the outer layer of DSF and simulation results provide a wide range of possibilities for energy performance. The studied case is an office building located in Tehran, the capital city of Iran, with the latitude and the longitude of 35.76° and 51.45°. This building consists of five floors with ten units and a total controlled area in terms of heating, cooling, ventilation, and air conditioning and it is 1625 square meters. Cooling and thermal loads are calculated as 134 and 213 kilowatts (kW), respectively. According to the simulation, the total nominal installation capacity of photovoltaic modules of the suggested configuration is 10 kW. According to the direction of the buildings, it receives more radiation from the southern part. In this respect, much of the cooling loss depends on the southern side. To quantify the effect of different geometrical shapes of the southern façade, this surface is divided into five parts including sections A, B, C, D, and E, as shown in Figure 1, and it includes a front view of the existing façade, proposed outer façade as a retrofit solution, and a side view of the outer façade for summer and winter cases.

The research team aims to identify the impact of the system in both chimney and blanket modes. The system would have an impact in terms of energy saving both in the summer and winter cases. Accordingly, the research team intends to review the technical impact of the suggested structure in terms of energy efficiency and the outer façade has been simulated such that occupants in the building can see the outer side of the existing window through another window. Therefore, in the simulated outer façade, there are photovoltaic modules parallel to the wall for the inner façade and there are windows parallel to the windows. The geometry of sections A, C, and E provides proper ground for the application of both glass and PV modules as the outer façade. Glass can be used in parallel to glass windows of the existing façade and PV modules may be applied in parallel to the connecting small walls between levels. Due to the geometry of sections B and D for the existing façade which is a wall, the suggested outer façade is shaped by an integrated PV module wall. A detailed descriptive view of the existing façade with the proposed glass and photovoltaic outer façade is given in Figure 1.

2. MATERIALS AND METHODS

In this section, the theory of formulation behind the stated problem is clarified. Thereafter, considering the assumptions on the solution of the problem, the applied tool for this procedure was defined. Finally, all the relevant input parameters were defined. To achieve the objective of analysis, all required heat transfer equations were determined. By considering the Solar Heat Gain Coefficient (SHGC) of glass and solar total radiation on a vertical surface, the heat transfer rate of glass-based outer skin was calculated through Equation (1). The wall surface heat transfer rate was calculated using Equation (2). The mean temperature of the boundary layer and the temperature coefficient of thermal conductivity were calculated through Equations (3) and (4), respectively [26, 27].

$$q_w = SHGC \times G_{tV} = h_{conv_w} \times (T_w - T_{amb}) \quad (1)$$

$$q_{wall} = G_{tV} = h_{conv_{wall}} \times (T_{wall} - T_{amb}) \quad (2)$$

$$T_f = \frac{T_w + T_{amb}}{2} \text{ or } \frac{T_{Tedlar} + T_{amb}}{2} \quad (3)$$

$$\beta = \frac{1}{T_f + 273.15} \quad (4)$$

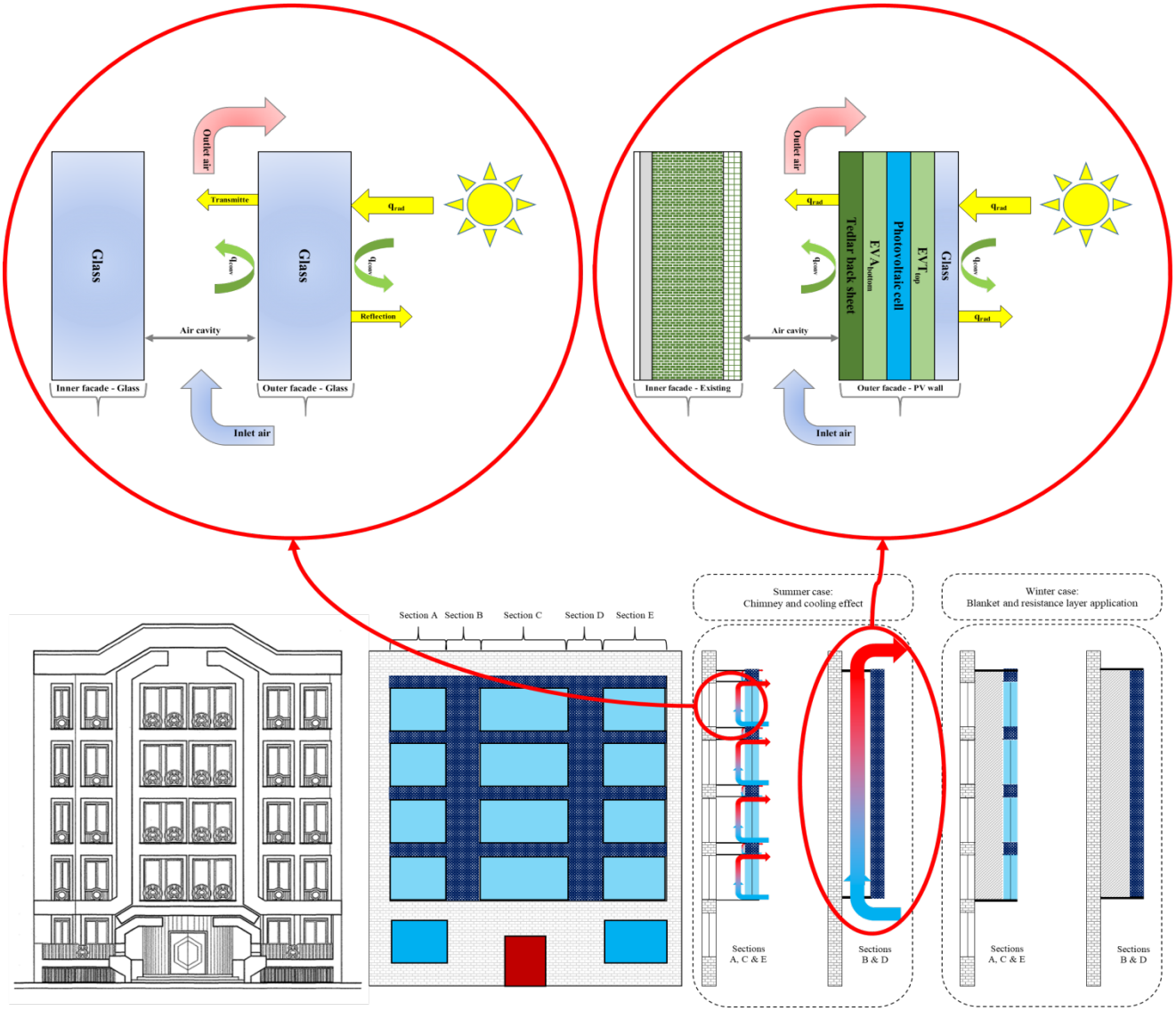

Figure 1. Front view of the existing facade (left bottom) and proposed outer facade as a retrofit solution (middle bottom); side view of outer façade for summer and winter cases (right bottom); side view of double façade with outer window wall (left top) and double façade with outer PV wall (right top).

Be keeping the amount of wind velocity and ambient temperature in mind, free convection heat transfer coefficient of outer skin outside and sky temperature were calculated through the experimental equations (5) and (6) [7, 28]. Temperatures of different photovoltaic layers were determined using energy balance equations by Equations (7) to (11) [29].

$$h_{conv_t} = 2.8+(3\times V_{wind}) \quad (5)$$

$$T_{sky} = \left(0.037536\times T_{amb}^{\,1.5}\right)+(0.32\times T_{amb}) \quad (6)$$

$$h_{conv_t}\left(T_{amb}-T_g\right)+\varepsilon_g F\sigma\left(T_{sky}^{\,4}-T_g^{\,4}\right) +\alpha_g G_{tV}-k_g\frac{T_g-T_{EVA_t}}{l_g}=0 \quad (7)$$

$$k_g\frac{T_g-T_{EVA_t}}{l_g}-k_{EVA_t}\frac{T_{EVA_t}-T_{cell}}{l_{EVA_t}}+\tau_g\alpha_{EVA}G_{tV}=0 \quad (8)$$

$$k_{EVA_t}\frac{T_{EVA_t}-T_{cell}}{l_{EVA_t}}-k_{EVA_b}\frac{T_{cell}-T_{EVA_b}}{l_{EVA_b}} +\tau_g\tau_{EVA}\left(\alpha_{cell}K+\alpha_{EVA}\left(1\text{-}K\right)\right)G_{tV}-\eta_{cell}G_{tV}=0 \quad (9)$$

$$k_{EVA_b}\frac{T_{cell}-T_{EVA_b}}{l_{EVA_b}}-k_{Tedlar}\frac{T_{EVA_b}-T_{Tedlar}}{l_{Tedlar}} +\tau_g\tau_{EVA}\tau_{EVA}\alpha_{Tedlar}\left(1\text{-}K\right)G_{tV}=0 \quad (10)$$

$$-h_{conv_{b\_PV}}\left(T_{Tedlar}-T_{amb}\right)+\varepsilon_{Tedlar}F\sigma\left(T_{Tedlar}^{\,4}-T_{amb}^{\,4}\right) +k_{Tedlar}\frac{T_{EVA_b}-T_{Tedlar}}{l_{Tedlar}}=0 \quad (11)$$

The selected photovoltaic (PV) module is of mono-crystalline type and it is characterized by better efficiency and greater popularity in Tehran for the integrated applications to buildings. The actual efficiency of the photovoltaic cell was calculated using the reference Equation (12) [30].

Heat transfer rate of PV module Tedlar surface was calculated through Equation (13). Properties of air including thermal conductivity, dynamic viscosity, density, kinematic viscosity, and Prandtl number for a cavity between two façades were determined using the corresponding tables. Modified Grashof number for constant heat flux was calculated through Equation (14) [26, 27].

$$\eta_{cell} = \eta_{ref}\left[1-\beta_{ref}\left(T_{cell}-T_{ref}\right)\right] \quad (12)$$

$$q_{Tedlar} = h_{conv_{b\_PV}} \times (T_{Tedlar} - T_{amb}) \quad (13)$$

$$Gr^* = \frac{\beta g q_w L^4}{k\gamma^2} \text{ or } Gr^* = \frac{\beta g q_{Tedlar} L^4}{k\gamma^2} \quad (14)$$

Finally, Nusselt number and natural convention heat transfer coefficient in the cavity boundary condition were calculated using Equations (15) and (16) for laminar flow and using Equations (17) and (18) for turbulent flow [26, 27].

$$10^5 < Gr^* Pr < 10^{11} \rightarrow Nu_x = 0.6 \times \left(Gr^* Pr\right)^{0.2} \quad (15)$$

$$h_m = 1.25 \times \frac{Nu_x k}{L} \quad (16)$$

$$2\times10^{13} < Gr^* Pr < 10^{16} \rightarrow Nu_x = 0.568 \times (Gr^* Pr)^{0.22} \quad (17)$$

$$h_m = 1.136 \times \frac{Nu_x k}{L} \quad (18)$$

Transport phenomenon was applied to thermal performance analysis of a studied building and to the development of a temperature and velocity profile for boundary conditions of the air cavity. Three main functions for the analysis including continuity, energy, and momentum equations are shown in Equations (19) to (21) [26, 27].

$$\frac{\partial u}{\partial x} + \frac{\partial \upsilon}{\partial y} = 0 \quad (19)$$

$$u\frac{\partial T}{\partial x} + \upsilon\frac{\partial T}{\partial y} = \frac{K}{\rho c_p}\frac{\partial^2 T}{\partial y^2} + \frac{\gamma}{c_p}\left(\frac{\partial u}{\partial y}\right)^2 \quad (20)$$

$$\rho\left(u\frac{\partial u}{\partial x} + \upsilon\frac{\partial u}{\partial y}\right) = \mu\frac{\partial^2 u}{\partial y^2} - \frac{\partial p}{\partial x} \quad (21)$$

The applied solution method for determining temperature and velocity profiles was the analytical method for both photovoltaic and glass as the external façade. Obtained temperature and velocity functions as well as rendered spacing and velocity functions for glass and PV outer skins were determined in Equations (22) to (25).

$$\frac{T_{(x,y)} - T_{amb}}{T_w \text{ or } T_{Tedlar} - T_{amb}} = \left(1-\frac{y}{\delta}\right)^2 \quad (22)$$

$$U_{(x,y)} = \left[U_0(x)\frac{\beta\delta^2 g}{4\gamma}\left(T_w \text{ or } T_{Tedlar} - T_{amb}\right)\right] \times \frac{y}{\delta}\left(1-\frac{y}{\delta}\right)^2 \quad (23)$$

$$\delta(x) = 3.93\left(0.952+Pr\right)^{0.25} \times \left[\frac{\beta g\left(T_w \text{ or } T_{Tedlar} - T_{amb}\right)}{\gamma^2}\right]^{-0.25} Pr^{-0.5} x^{0.25} \quad (24)$$

$$U_0(x) = 5.17\gamma\left(0.952+\frac{1}{Pr}\right)^{-0.5} \times \left[\frac{\beta g\left(T_w \text{ or } T_{Tedlar} - T_{amb}\right)}{\gamma^2}\right]^{0.5} x^{0.5} \quad (25)$$

Terms T_w and T_{Tedlar} must be used for glass-based and PV-based outer skins, respectively. Considering the geometry of the outer façade for different sections of the studied case, three situations need to be analyzed for developing temperature and velocity profiles below:

- Glass parts of sections A, C, and E: each section consists of four separate levels of glass façade with a height of 2.37 meters with different widths;
- PV parts of sections A, C, and E: each section consists of four separate levels of PV façade with a height of 0.53 meter with different widths;
- PV parts of sections B and D: each section consists of one integrated PV façade with a height of 12.5 meters with a similar width.

To compare the application of glass and PV façades and the existing inner façade in a critical condition, cooling and thermal losses were formulated. The effect of DSF in the summer case in a chimney was considered. In this situation, natural ventilation in the air cavity reduced the cooling load.

For calculation of this effect, Equations (26) to (29) were applied. By using Equations (26) and (27), the heat loss of the glass-based inner skin in the summer cases was obtained for single and double-façade modes, respectively. Through Equations (28) and (29), the heat loss of the wall-based inner skin in the summer cases was obtained for single and double-façade modes, respectively.

It should be noted that due to the complexity of the model, the impact of the windows frame was neglected within the analysis. Besides, the convective heat transfer in the air gap was disregarded in the winter case for simulation.

$$Q_{in_{w\_SS}} = SHGC \times G_{tV} A_{w_{in}} - h_{conv_w}\left(T_w - T_{in}\right)A_{w_{in}} - U_w\left(T_{amb} - T_{in}\right)A_{w_{in}} \quad (26)$$

$$Q_{in_{w\_DS}} = SHGC \times G_{tV} A_{w_{out}} - h_{conv_w}\left(T_w - T_{amb}\right)A_{w_{out}} - \bar{h}_m\left(\bar{T}_w - T_{in}\right)A_{w_{out}} - U_w\left(T_{critical} - T_{in}\right)A_{w_{in}} \quad (27)$$

$$Q_{in_{wall\_SS}} = G_{tV} A_{wall} - h_{conv_{wall}}\left(T_{wall} - T_{in}\right)A_{wall} - U_{wall}\left(T_{amb} - T_{in}\right)A_{wall} \quad (28)$$

$$Q_{in_{Pv\_DS}} = \varepsilon_{Tedlar} F\sigma\left(T_{Tedlar}^{\ 4} - T_{amb}^{\ 4}\right)A_{PV} - h_{conv_t}\left(T_g - T_{amb}\right)A_{PV} - \bar{h}_m\left(\bar{T}_{Tedlar} - T_{in}\right)A_{wall} - U_{wall}\left(T_{critical} - T_{in}\right)A_{wall} \quad (29)$$

On the other hand, for the winter case, the effect of DSF was considered as an extra thermal-resistant layer, which would reduce the heat loss from the inner side to the outside which is a so-called blanket mode. Using Equations (30) and (31), the heat loss of the glass-based inner skin in the winter cases was obtained in single and double-façade conditions, respectively. Using Equations (32) and (33), the heat loss of the wall-based inner skin in the winter case was obtained for single and double-façade modes, respectively.

$$Q_{out_{w\_SS}} = \frac{1}{R_{w\_SS}}\left(T_{in} - T_{amb}\right)A_{w_{in}} \quad (30)$$

$$Q_{out_{w\_SS}} = \frac{1}{R_{w\_SS}}\left(T_{in} - T_{amb}\right)A_{w_{in}} \quad (31)$$

$$Q_{out_{wall\_SS}} = \frac{1}{R_{wall\_SS}}\left(T_{in}\text{-}T_{amb}\right)A_{wall} \quad (32)$$

$$Q_{out_{PV\_DS}} = \frac{1}{R_{PV\_DS}}\left(T_{in}\text{-}T_{amb}\right)A_{PV} \quad (33)$$

Finally, Equations (34) and (35) were used for calculation of cooling and the thermal load reduction in critical seasonal conditions in the summer and winter cases, respectively.

$$Q_{in} = \left(Q_{in_{w\_SS}} - Q_{in_{w\_DS}}\right) + \left(Q_{in_{wall\_SS}} - Q_{in_{PV\_DS}}\right) \quad (34)$$

$$Q_{out} = \left(Q_{out_{w\_SS}}\text{-}Q_{out_{w\_DS}}\right) + \left(Q_{out_{wall\_SS}}\text{-}Q_{out_{PV\_DS}}\right) \quad (35)$$

To analyze the thermal energy performance of the proposed BIPVT-DSF, computerized code was developed using Engineering Equation Solver (EES) software. The procedure for running the mentioned code consists of five main steps as follows:

- Calculation of heat rate from outer to inner skin by analyzing input weather data and constant parameters;
- Assuming a convective heat transfer coefficient for the backside of the outer façade and calculation of all relevant heat transfer parameters including Nusselt and Grashof numbers for the boundary layer;
- Evaluation of convergence for calculated convective heat transfer coefficient and resulting temperature and velocity profiles for glass and photovoltaic outer façades;
- Providing the temperature and velocity profile following continuity, momentum, and energy equations;
- Calculation of cooling load and thermal load reductions as well as the amount of energy saving.

As the most benefits of DSF depend on the geographical positioning and the climatological condition of the building, it is necessary to review the application of DSF according to the critical seasonal conditions. All input parameters of critical condition for the summer case as well as constant parameters relevant to the geometry of outer façade and physical properties are shown in Table 1.

Input parameters are given in Table 2 that include surface areas, overall heat transfer coefficients, thermal resistance values, and ambient and seasonal comfort temperatures. Simulation outputs are presented in the results and discussion section.

Table 1. Input parameters and weather information in the critical condition.

Parameter (unit)	Value
Acceleration due to gravity: g (m/s^2)	9.81
Absorptivity of PV module ethylen vinyl asetat (EVA) layer: α_{EVA}	0.03
Absorptivity of PV module glass layer: α_g	0.02
Absorptivity of PV module photovoltaic cell layer: α_{cell}	1
Absorptivity of PV module Tedlar layer: α_{Tedlar}	1
Ambient temperature: T_{amb} (°C)	40.4
Cavity depth: Δ (m)	0.3
Efficiency of the PV module at the standard test condition: η_{ref}	0.1496
Emissivity of PV module glass layer: ε_g	0.91
Emissivity of PV module Tedlar layer: ε_{Tedlar}	0.85
Length of outer façade for photovoltaic sections A, C & E: L (m)	0.53
Length of outer façade for photovoltaic sections B & D: L (m)	12.5
Length of outer façade for windows sections A, C & E: L (m)	2.37
Packing factor of PV module: K	0.9
Solar heat gain coefficient: SGHC	0.42
Solar total radiation on a vertical surface: G_{tV} (W/m^2)	619.2
Stefan–Boltzmann constant: σ ($W/m^2.K^4$)	5.67×10^{-8}
Temperature coefficient of PV module: β_{ref}	0.0045
Temperature of PV module at standard test condition: T_{ref} (°C)	25
Thermal conductivity coefficient of PV module ethylene vinyl acetate (EVA) layer: k_{EVA} (W/m.K)	0.35
Thermal conductivity coefficient of PV module glass layer: k_g (W/m.K)	1.8
Thermal conductivity coefficient of PV module Tedlar layer: k_{Tedlar} (W/m.K)	0.3
Thickness of PV module ethylene vinyl acetate (EVA) layer: l_{EVA} (m)	0.0004
Thickness of PV module glass layer: l_g (m)	0.004
Thickness of PV module Tedlar layer: l_{Tedlar} (m)	0.0003
Transmission coefficient of PV module ethylen vinyl asetat (EVA) layer: τ_{EVA}	0.97
Transmission coefficient of PV module glass layer: τ_g	0.88
View factor: F	0.5
Wind velocity: V_{wind} (m/s)	3.8
Solar total radiation on a vertical surface: G_{tV} (W/m^2)	619.2

Table 2. Input parameters for calculation of cooling and thermal losses.

Parameter (unit)	Value
Ambient temperature in critical condition of a summer case: T_{amb} (°C)	40.4
Ambient temperature in critical condition of a winter case: T_{amb} (°C)	-4.6
Comfort temperature set for a summer case: T_{in} (°C)	21
Comfort temperature set for a winter case: T_{in} (°C)	18
Single-façade overall heat transfer coefficient for glass inner skin: U_w ($W/m^2.K$)	1.95
Single-façade overall heat transfer coefficient for wall inner skin: U_{wall} ($W/m^2.K$)	0.95

Surface area for glass inner façade: A_{w_in} (m^2)	102.38
Surface area for glass outer façade: A_{w_out} (m^2)	102.38
Surface area for PV outer façade for sections A, C & E: A_{PV_2} (m^2)	20.29
Surface area for PV outer façade for sections B & D: A_{PV_1} (m^2)	39.75
Surface area for wall inner façade: A_{wall} (m^2)	60.04
Thermal resistance for single-façade glass inner skin in winter case: R_{w_SS} (m^2.K/W)	0.512
Thermal resistance for double-façade glass outer skin in winter case: R_{w_DS} (m^2.K/W)	1.2
Thermal resistance for double-façade PV outer skin in winter case: R_{PV_DS} (m^2.K/W)	1.236
Thermal resistance for single-façade wall inner skin in winter case: R_{wall_SS} (m^2.K/W)	1.05

3. RESULTS AND DISCUSSION

Initial obtained results include thermal properties, Nusselt and Grashof numbers, natural convection heat transfer coefficients, rendered spacing for the boundary layer, and velocity in the initial condition for glass and PV façades, and they are tabulated in Table 3.

Results must be analyzed for both summer and winter case applications. Given the system description of the studied case, DSF was considered as a chimney in the summer case and as a blanket in the winter case.

A comparison of temperature values for the outer façade of glass and PV-based skins showed that the glass façade had higher values than the PV façade. The other important factor is the natural convection heat transfer coefficient which is lower in PV parts than glass parts. Therefore, it is expected that the glass façade will have a higher impact on cooling load reduction. Due to the geometrical difference of three parts, the spacing of the boundary layer varies between 2.08 to 4.59 centimeters.

Table 3. Simulation obtained results for three different status of outer façade.

Parameter (unit)	Window (sections A, C & E)	Photovoltaic (sections A, C & E)	Photovoltaic (sections B & D)
Cavity depth: Δ (m)	0.241	0.234	0.234
Free convection heat transfer coefficient: $h_{conv,t}$ (W/m^2.K)	-	14.2	14.2
Glass based outer skin heat transfer rate: q_w (W/m^2)	260	-	-
Kinematic viscosity of air: γ (m^2/s)	0.0000186	0.0000185	0.0000186
Mean temperature for boundary layer between inner surface and cavity: T_f (°C)	61.2	52.57	52.77
Modified Grashof number for constant heat flux: Gr*	2.4888×10^{13}	2.7153×10^{10}	7.9893×10^{15}
Natural convection heat transfer coefficient: h_x (W/m^2.K)	5.49	3.57	3.68
Natural convection heat transfer coefficient for laminar or turbulent flow: h_m (W/m^2.K)	6.24	4.45	4.18
Nusselt number for laminar or turbulent flow: Nu_x	539.04	68.65	1666.54
Photovoltaic cell efficiency: η_{cell}	-	0.1229	0.1226
Prandtl number of air: Pr	0.721	0.7223	0.722
PV module Tedlar surface hear transfer rate: q_{Tedlar} (W/m^2)	-	108.32	103.38
Rendered spacing function based on initial and boundary conditions: δ (m)	0.0278	0.0208	0.0459
Sky temperature: T_{sky} (°C)	-	22.57	22.57
Temperature coefficient of thermal conductivity: β (1/K)	0.002991	0.00307	0.003068
Temperature of PV module bottom EVA layer: $T_{EVA,\,b}$ (°C)	-	64.77	65.15
Temperature of PV module glass layer: T_g (°C)	-	63.25	63.61
Temperature of PV module photovoltaic cell layer: T_{cell} (°C)	-	64.73	65.11
Temperature of PV module top EVA layer: $T_{EVA,\,t}$ (°C)	-	64.24	64.61
Temperature of PV module Tedlar layer: T_{Tedlar} (°C)	-	64.74	65.13
Temperature on the wall outside surface: T_{wall} (°C)	-	84	84
Temperature on the windows outside surface: T_w (°C)	82	-	-
Thermal conductivity coefficient: k (W/m.K)	0.02782	0.02757	0.02758
Velocity function for boundary conditions: U_0 (m/s)	6.18	2.12	10.32

To investigate the shape of temperature and velocity profiles for three sections of the outer façade, three and two-dimensional graphs were illustrated using EES software considering the initial cavity depth of 0.3 meter. Following the identification of the appropriate cavity depth, comparative integrated temperature and velocity profiles were demonstrated for inlet and outlet positions of each of three parts. Temperature and velocity profiles for glass and PV-based different sections of the outer façade are shown in Figures 2 to 7.

By comparing temperature and velocity profiles, it is understandable that both material and geometrical characteristics of the outer façade will have an impact on the thermal performance of DSF. As a meaningful result of the analysis, the maximum temperature at the outlet of a cavity will be reduced in the case of larger heights. However, the maximum velocity at the outlet of a cavity reduced at smaller heights. Given that temperature profiles and cavity depth have a significant impact on the thermal performance of a cavity, sensitivity analysis of these parameters must be investigated for analyzing the thermal energy performance of the retrofit solution.

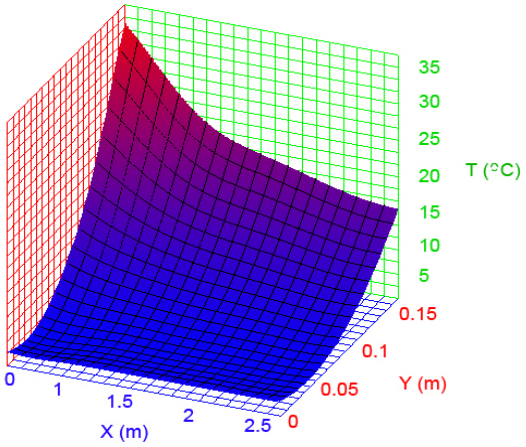

Figure 2. Temperature profile-sections A, C & E (glass).

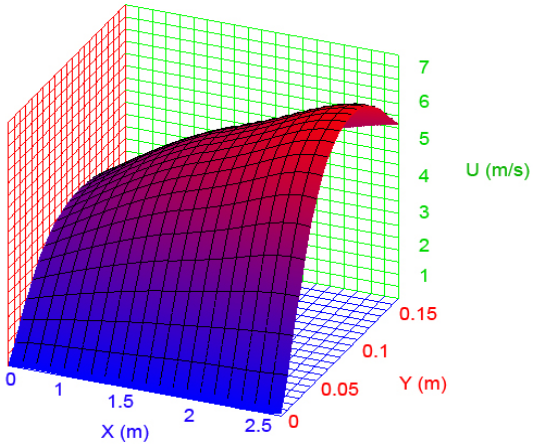

Figure 3. Velocity profile-sections A, C & E (glass).

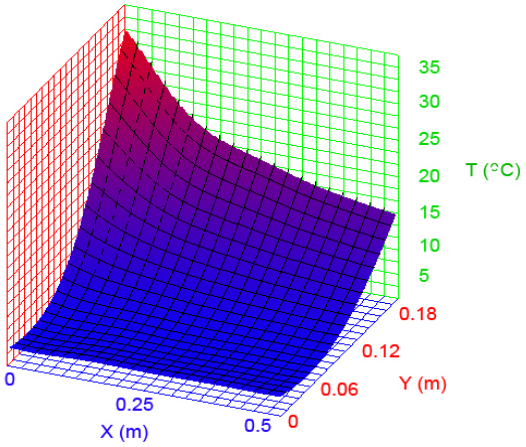

Figure 4. Temperature profile-sections A, C & E (PV).

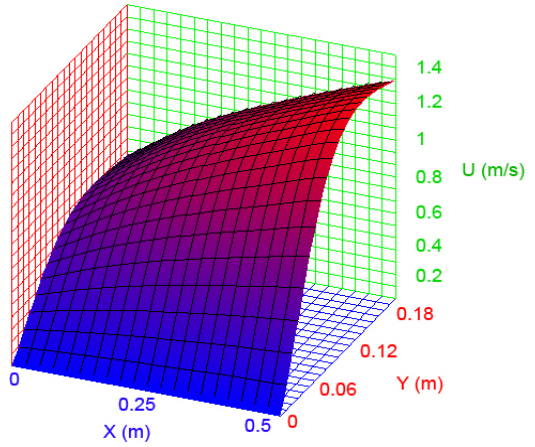

Figure 5. Velocity profile-sections A, C & E (PV).

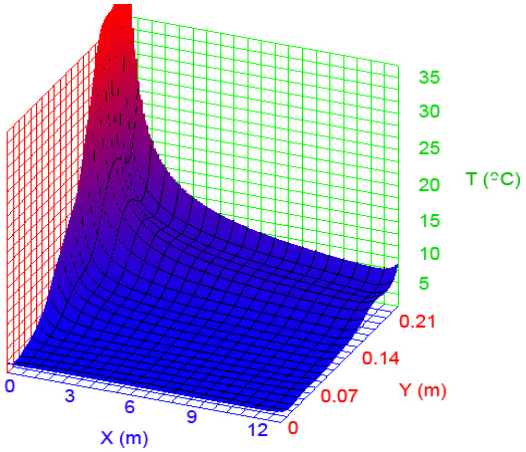

Figure 6. Temperature profile-sections B & D (PV).

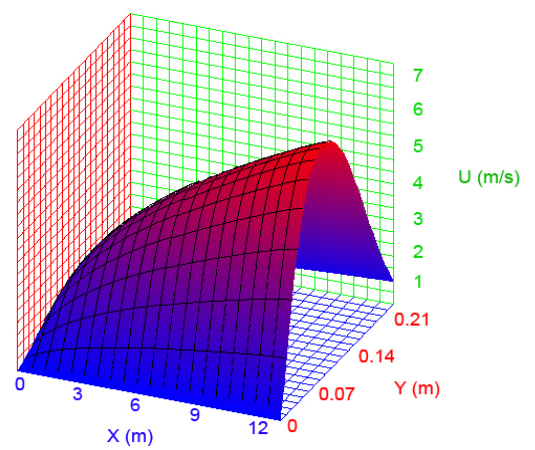

Figure 7. Velocity profile-sections B & D (PV).

According to the assumptions of this study, there are two temperature control strategies including:

- Temperature control on the inner side of the building as a comfort temperature protocol;
- Temperature control on the air gap between inner and outer façades.

For the first case strategy, it is assumed that the demand side will be responsible for keeping the comfort temperature as constant as possible. For the second case strategy, air temperature at skin spacing should be assumed to be at least 5 °C less than the ambient temperature for the summer case to prevent the crisis at the temperature profile through façades. Thus, it is required to investigate at what depth of the cavity will this crisis be averted for each of the outer façade modes. According to the simulation results, the temperature crisis occurs at a cavity depth of 8.35 centimeters at the inlet of the glass-based façade and at 9.37 centimeters, at the inlet of PV-based sections A, C, and E, and at 9.35 centimeters at the inlet of PV-based sections B and D. Simulation results show the appropriate cavity depth for glass-based and PV-based sections A, C, and E as well as the outer façades of sections B and D must be 21.65, 20.63 and 20.65 centimeters, respectively.

At the next step, comparative integrated temperature and velocity profiles were demonstrated for inlet and outlet positions in Figure 8.

A comparison of temperature and velocity profiles shows the proper application of DSF based on simulations. In accordance with the temperature profiles, outlet temperature reduced significantly in comparison to the inlet temperature in all cases, which led to less cooling load on mechanical or electrical devices due to natural cooling facilitated by the application of the outer façade. However, the effect of DSF was significant in sections B and D with the application of PV in terms of reduction in temperature, mainly due to the height of the outer wall. Although the results of the analysis for sections B and D are interesting, the effects of all elements on sections A, C, and E for glass-based and PV-based cases must be considered to properly conclude the results. This is because all the illustrated graphs are for one segment of each section.

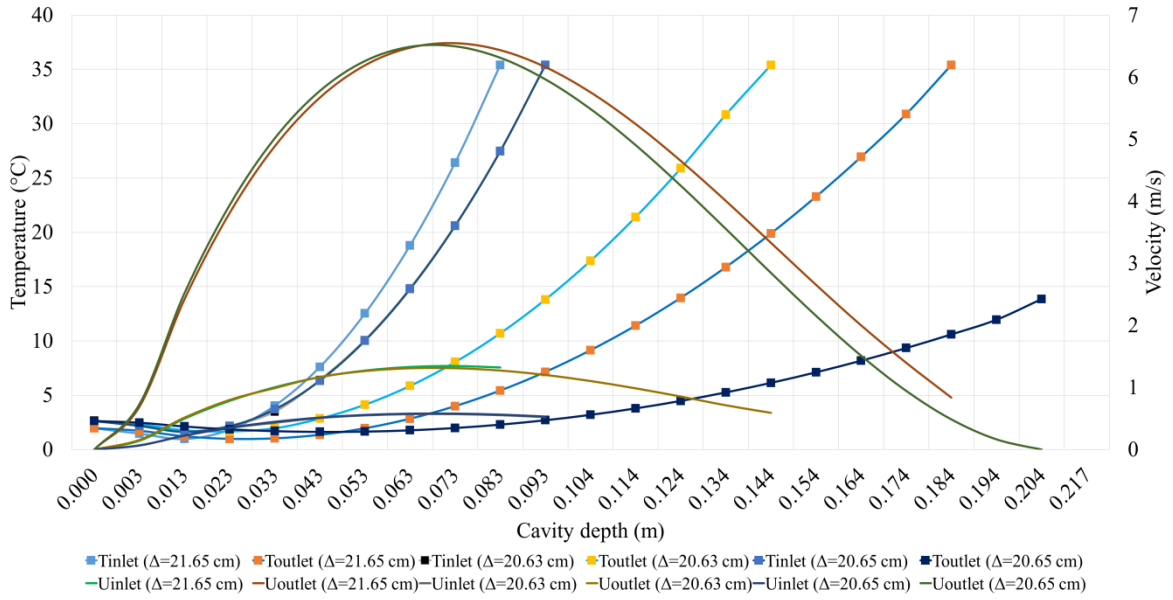

Figure 8. Temperature and velocity profiles for inlet and outlet of sections.

According to the results, DSF with the proposed configuration had a notable role in reducing the cooling demand and thermal load in the summer and winter cases by 18.5 kW and 2.79 kW, respectively, which were not considered in comparison to the summer case. In this respect, DSF had a significant effect on cooling load reduction by 8.7 percent and it managed to reduce the thermal load by 2.1 percent. All of the above results were provided with emphasis on the comfort temperatures of 21 and 18 °C for summer and winter, respectively.

In fact, there is a great potential for greater energy saving if comfort temperature set points would be adjusted as high as possible in the summer case and in reverse in the winter case. Table 4 shows the amount of cooling and thermal load reductions considering different comfort set points at a constant PV to glass façade surface ratio (58.6 %).

If the comfort indoor set point for summer cases varies between 18 and 24 °C, the total cooling load reduction will increase from 14.2 to 22.7 kW. In the winter case, if the comfort indoor set point varies between 15 and 21 °C, the total thermal load reduction will increase from 2.42 to 3.16 kW.

According to Table 4, the share of glass-based and PV-based façades on total cooling load reduction does not have a significant difference. However, the glass façade has by far greater impact on the reduction of the total thermal load than the PV façade. Besides, both glass and PV façades have a greater effect in summer cases compared to the winter case; however, the impact of the PV façade is more considerable in the summer case than that in the winter case.

The other important factor with a significant effect on cooling and thermal load reduction is the area ratio on the

outer façade which can be defined based on a variation of PV surface area divided by glass surface area. Table 5 demonstrates the effect of different area ratios on cooling and thermal load reduction.

Higher more area ratio results in a more significant reduction in the total cooling load and an insignificant decrease in the thermal load. However, slopes of cooling and thermal load reduction are significantly smaller than the area ratio. Of course, the application of more PV modules than a glass façade will result in a greater cooling load reduction at a constant comfort temperature (21 degrees Celsius). On the other hand, the application of more PV modules in comparison to the glass façade results in a lower thermal load reduction in the winter case.

Table 4. Cooling and thermal load reductions at different indoor temperature set points.

Inner side temperature (°C)	**15**	**18**	**21**	**24**
Cooling load reduction for windows section (kW)	-	7.36	9.81	12.3
Cooling load reduction for photovoltaic section (kW)	-	6.86	8.65	10.4
Total cooling load reduction (kW)	-	14.2	18.5	22.7
Thermal load reduction for windows section (kW)	2.25	2.6	2.94	-
Thermal load reduction for photovoltaic section (kW)	0.17	0.19	0.22	-
Total thermal load reduction (kW)	2.42	2.79	3.16	-
Inner side temperature (°C)	15	18	21	24
Cooling load reduction for windows section (kW)	-	7.36	9.81	12.3

Table 5. Cooling and thermal load reduction at different area ratios (photovoltaic to glass).

Photovoltaic area to windows area ratio (%)	**32.4**	**39.5**	**49.8**	**58.6**
Cooling load reduction for windows section (kW)	11.75	11.15	10.38	9.8
Cooling load reduction for photovoltaic section (kW)	5.73	6.63	7.78	8.65
Total cooling load reduction (kW)	17.47	17.78	18.16	18.46
Thermal load reduction for windows section (kW)	3.11	2.96	2.75	2.6
Thermal load reduction for photovoltaic section (kW)	0.13	0.15	0.17	0.19
Total thermal load reduction (kW)	3.24	3.1	2.93	2.79

4. CONCLUSIONS

The present study analyzed the thermal energy performance of the building integrated photovoltaic thermal double-skin façade (BIPVT-DSF) system using glass-based and photovoltaic-based façades as the outer façade for an existing building in Tehran city, located in the Middle East climate condition. To identify the amount of reduction in cooling and thermal loads through the suggested system, thermal performance analysis was conducted by using code development in EES software. The solution method was based on an analytical approach using heat transfer and thermodynamics phenomenon.

In accordance with the aim of this research study, a solution was provided using an analytical approach and the temperature and velocity profiles for different scenarios were investigated. The application of this approach led to analysis of the differences between glass-based and PV-based outer façades. Thus, the research team used the analysis results to compare the impact of glass-based and PV-based outer façades on cooling and thermal loads reduction and energy saving. According to the results, outlet temperature reduced significantly compared to the inlet temperatures in all of the reviewed cases.

Based on the quantitative results of the study, the proposed DSF had great impact on reducing cooling demand in the summer case by 18.5 kW reduction. However, the amount of thermal load reduction, i.e., 2.79 kW, in the winter case was not considerable. In doing so, DSF reduced cooling and thermal loads by 8.7 and 2.1 %, respectively.

Thereafter, the impact of variation of comfort indoor set points for the summer and winter cases with the application of BIPVT-DSF was reviewed. Finally, the effect of variation of PV to glass surface area on cooling and thermal load reduction was evaluated. Sensitivity analysis showed that both glass and PV façades had a greater impact in the summer case than those in the winter case. Additionally, the impact of the PV façade was more considerable in the summer case than that in the winter season. The building sector was considered as one of the key energy sectors in Iran with the Middle Eastern climate condition. Since Iran is facing a new challenge of the electricity demand peak load in the summer case, the suggested system can be considered within the process of building retrofit solution.

According to the results of this study, the proposed BIPVT-DSF system is an appropriate energy saving measure from the technical perspective mostly in the summer case. Therefore, if the government or the investors of the construction industry can consider the financial feasibility of this energy saving measure in their plans, it is worthwhile to apply this system to some parts of the existing buildings and some others for the new designs. Therefore, some part of the electricity demand in the summer case was reduced.

5. ACKNOWLEDGEMENT

This research was supported by the Iranian Fuel Conservation Company (IFCO). Authors appreciate colleagues of the research and development department as well as energy optimization at the building department who provided insight and expertise that assisted the research.

NOMENCLATURE

A_{PV}	Surface area for PV outer façade (m^2)
A_{w_in}	Surface area for glass inner façade (m^2)
A_{w_out}	Surface area for glass outer façade (m^2)
A_{wall}	Surface area for wall inner façade (m^2)
c_p	Specific heat at constant pressure (kJ/kg.K)
F	View factor
g	Acceleration due to gravity (m/s^2)
Gr*	Modified Grashof number for constant heat flux
G_{tV}	Solar total radiation on a vertical surface (W/m^2)
h_{conv}	Free convection heat transfer coefficient ($W/m^2.K$)
h_m	Natural convection heat transfer coefficient for laminar or turbulent flow ($W/m^2.K$)
$\bar{h}$	Average natural convection heat transfer coefficient ($W/m^2.K$)
k	Thermal conductivity coefficient (W/m.K)
K	Packing factor of PV module
L	Wall length for PV or windows as outer façade (m)
l	Thickness (m)
Nu_x	Nusselt number for laminar or turbulent flow
p	Pressure (kPa)
Pr	Prandtl number of air
Q_{in}	Cooling load reduction in critical temperature of summer case with the application of double façade (kW)
$Q_{in_{PV\_DS}}$	Double-façade heat loss for PV outer skin in summer case (W)
$Q_{in_{w\_DS}}$	Double-façade heat loss for glass outer skin in summer case (W)
$Q_{in_{w\_SS}}$	Single-façade heat loss for glass inner skin in summer case (W)
$Q_{in_{wall\_SS}}$	Single-façade heat loss for wall inner skin in summer case (W)
Q_{out}	Thermal load reduction in critical temperature of winter case with the application of double façade (kW)
$Q_{Out_{PV\_DS}}$	Double-façade heat loss for PV outer skin in winter case (W)
$Q_{Out_{w\_DS}}$	Double-façade heat loss for glass outer skin in winter case (W)
$Q_{Out_{w\_SS}}$	Single-façade heat loss for glass inner skin in winter case (W)
$Q_{Out_{wall\_SS}}$	Single-façade heat loss for wall inner skin in winter case (W)
q_{Tedlar}	PV module Tedlar surface hear transfer rate (W/m^2)
q_w	Glass-based outer skin heat transfer rate (W/m^2)
R_{PV_DS}	Thermal resistance for double-façade PV outer skin in winter case ($m^2.K/W$)
R_{w_DS}	Thermal resistance for double-façade glass outer skin in winter case ($m^2.K/W$)
R_{w_SS}	Thermal resistance for single-façade glass inner skin in winter case ($m^2.K/W$)
R_{wall_SS}	Thermal resistance for single-façade wall inner skin in winter case ($m^2.K/W$)
SHGC	Solar heat gain coefficient
T	Temperature (°C or K)
T (x, y)	Two-dimensional temperature profile (°C)
T_{amb}	Ambient temperature (°C)
T_f	Mean temperature for boundary layer between inner surface and cavity (°C or K)
T_{in}	Comfort temperature set for summer or winter case (°C)
T_{ref}	Temperature of PV module at standard test condition (°C)
T_{sky}	Sky temperature (°C or K)
u	velocity (x coordinate) (m/s)
U (x, y)	Two-dimensional velocity profile (m/s)
U_0	Velocity function for boundary conditions (m/s)
U_w	Single-façade overall heat transfer coefficient for glass inner skin ($W/m^2.K$)
U_{wall}	Single-façade overall heat transfer coefficient for wall inner skin ($W/m^2.K$)
V_{wind}	Wind velocity (m/s)
x, y	Coordinates in the Cartesian system (m)

Greek letters

α	Absorptivity
β	Temperature coefficient of thermal conductivity (1/K)
β_{ref}	Temperature coefficient of PV module
γ	Kinematic viscosity of air (m^2/s)
Δ	Cavity depth (m)
δ	Rendered spacing function based on initial and boundary conditions (m)
ε	Emissivity of PV module glass surface
η_{cell}	Photovoltaic cell efficiency
η_{ref}	Efficiency of the PV module in the standard test condition
μ	Dynamic viscosity of air (kg/m.s)
ρ	Density of air (kg/m^3)
σ	Stefan–Boltzmann constant ($W/m^2.K^4$)
τ	Transmission coefficient
ν	velocity (y coordinate) (m/s)

Subscripts

cell	PV module cell
DS	Double skin
EVA, b	PV module bottom EVA layer
EVA, t	PV module EVA top layer
g	PV module glass
PV	Photovoltaic panel
SS	Single-skin
Tedlar	PV module Tedlar back sheet
w	Building windows façade
wall	Building wall façade

REFERENCES

1. Lai, C. and Hokoi, S., "Solar façades: A review", ***Building and Environment***, Vol. 91, (2015), 152-165. (https://doi.org/10.1016/j.buildenv.2015.01.007).
2. Agathokleous, R.A. and Kalogirou, S.A., "Double skin facades (DSF) and building integrated photovoltaics (BIPV): A review of configurations and heat transfer characteristics", ***Renewable Energy***, Vol. 89, (2016), 743-756. (https://doi.org/10.1016/j.renene.2015.12.043).
3. Darkwa, J., Li, Y. and Chow, D.H.C., "Heat transfer and air movement behaviour in a double-skin façade", ***Sustainable Cities Society***, Vol. 10, (2014), 130-139. (https://doi.org/10.1016/j.scs.2013.07.002).
4. Kant, K., Shukla, A., Sharma, A. and Biwole, P.H., "Thermal response of poly-crystalline silicon photovoltaic panels: Numerical simulation and experimental study", ***Solar Energy***, Vol. 134, (2016), 147-155. (https://doi.org/10.1016/j.solener.2016.05.002).
5. Atkin, P. and Farid, M.M., "Improving the efficiency of photovoltaic cells using PCM infused graphite and aluminum fins", ***Solar Energy***, Vol. 114, (2015), 217-228. (https://doi.org/10.1016/j.solener.2015.01.037).
6. Lai, C. and Chen, R.H., "Novel heat dissipation design incorporating heat pipes for DC combiner boxes of a PV system", ***Solar Energy***, Vol. 85, No. 9, (2011), 2053-2060. (https://doi.org/10.1016/j.solener.2011.05.013).
7. Kant, K., Shukla, A., Sharma, A. and Biwole, P.H., "Heat transfer studies of photovoltaic panel coupled with phase change material", ***Solar Energy***, Vol. 140, (2016), 151-161. (https://doi.org/10.1016/j.solener.2016.11.006).
8. Elarga, H., Goia, F., Zarrella, A., Dal Monte, A. and Benini, E., "Thermal and electrical performance of an integrated PV-PCM system in double skin façades: A numerical study", ***Solar Energy***, Vol. 136, (2016), 112-124. (https://doi.org/10.1016/j.solener.2016.06.074).
9. Zogou, O. and Stapountzis, H., "Energy analysis of an improved concept of integrated PV panels in an office building in central Greece", ***Applied Energy***, Vol. 88, No. 3, (2011), 853-866. (https://doi.org/10.1016/j.apenergy.2010.08.023).
10. Rabani, R., Faghih, A.K., Rabani, M. and Rabani, M., "Numerical simulation of an innovated building cooling system with combination of solar chimney and water spraying system", ***Heat and Mass Transfer***,

Vol. 50, No. 11, (2014), 1609-1625. (https://doi.org/10.1007/s00231-014-1366-5).

11. Corbin, C.D. and Zhai, Z.J., "Experimental and numerical investigation on thermal and electrical performance of a building integrated photovoltaic-thermal collector system", ***Energy and Buildings***, Vol. 42, No. 1, (2010), 76-82. (https://doi.org/10.1016/j.enbuild.2009.07.013).
12. Shakouri, M., Golzari, S. and Zamen, M., "Energy and exergy optimization of water cooled thermal photovoltaic (PV/T) system using genetics algorithm", ***Journal of Solar Energy Research***, Vol. 1, No. 1, (2016), 45-51.
13. Shakouri, M., Noorpoor, A., Golzari, S. and Zamen, M., "Energy simulation and parametric analysis of water cooled photovoltaic/thermal system", ***Amirkabir Journal of Mechanical Engineering***, Vol. 50, No. 6, (2018), 435-438. (https://doi.org/10.22060/mej.2017.12703.5402).
14. Pantic, S., Candanedo, L. and Athienitis, A.K., "Modeling of energy performance of a house with three configurations of building-integrated photovoltaic/thermal systems", ***Energy and Buildings***, Vol. 42, No. 10, (2010), 1779-1789. (https://doi.org/10.1016/j.enbuild.2010.05.014).
15. Cappelletti, F., Prada, A., Romagnoni, P. and Gasparella, A., "Passive performance of glazed components in heating and cooling of an open-space office under controlled indoor thermal comfort", ***Building and Environment***, Vol. 72, (2014), 131-144. (https://doi.org/10.1016/j.buildenv.2013.10.022).
16. Serra, V., Zanghirella, F. and Perino, M., "Experimental evaluation of a climate facade: energy efficiency and thermal comfort performance", ***Energy and Buildings***, Vol. 42, No. 1, (2010), 50-62. (https://doi.org/10.1016/j.enbuild.2009.07.010).
17. Ghadimi, M., Ghadamian, H., Hamidi, A.A., Shakouri, M. and Ghahremanian, S., "Numerical analysis and parametric study of the thermal behavior in multiple-skin façades", ***Energy and Buildings***, Vol. 67, (2013), 44-55. (https://doi.org/10.1016/j.enbuild.2013.08.014).
18. Fuliotto, R., Cambuli, F., Mandas, N., Bacchin, N., Manara, G. and Chen, Q., "Experimental and numerical analysis of heat transfer and airflow on an interactive building façade", ***Energy and Buildings***, Vol. 42, No. 1, (2010), 23-28. (https://doi.org/10.1016/j.enbuild.2009.07.006).
19. Kuznik, F., Catalina, T., Gauzere, L., Woloszyn, M. and Roux, J., "Numerical modelling of combined heat transfers in a double skin façade full-scale laboratory experiment validation", ***Applied Thermal Engineering***, Vol. 31, No. 14-15, (2011), 3043-3054. (https://doi.org/10.1016/j.applthermaleng.2011.05.038).
20. Mulyadi, R., Yoon, G. and Okumiya, M., "Study on solar heat gain and thermal transmittance of east and west-facing double-skin façade in hot and humid climate", ***AIJ Journal of Technology and Design***, Vol. 18, No. 40, (2012), 989-994. (https://doi.org/10.3130/aijt.18.989).
21. Hoseinzadeh, S., Zakeri, M.H., Shirkhani, A. and Chamkha, A.J., "Analysis of energy consumption improvements of a zero-energy building in a humid mountainous area", ***Journal of Renewable and Sustainable Energy***, Vol. 11, No. 1, (2019). (https://doi.org/10.1063/1.5046512).
22. Hoseinzadeh, S., "Thermal performance of electrochromic smart window with nanocomposite structure under different climates in Iran", ***Micro and Nanosystems***, Vol. 11, No. 2, (2019), 154-164. (https://doi.org/10.2174/1876402911666190218145433).
23. Hoseinzadeh, S. and Azadi, R., "Simulation and optimization of a solar-assisted heating and cooling system for a house in Northern of Iran". ***Journal of Renewable and Sustainable Energy***, Vol. 9, No. 4, (2017). (https://doi.org/10.1063/1.5000288).
24. Yousef Nezhad, M.E. and Hoseinzadeh, S., "Mathematical modelling and simulation of a solar water heater for an aviculture unit using MATLAB/SIMULINK", ***Journal of Renewable and Sustainable Energy***, Vol. 9, No. 6, (2017). (https://doi.org/10.1063/1.5010828).
25. Ghadamian, H., Ghadimi, M., Shakouri, M., Moghadasi, M. and Moghadasi, M., "Analytical solution for energy modeling of double skin façades building", ***Energy and Buildings***, Vol. 50, (2012), 158-165. (https://doi.org/10.1016/j.enbuild.2012.03.034).
26 Holman, J.P. and White, P.R.S., Heat transfer, 7th Ed., McGraw-Hill, UK, (1992).
27. Incoropera, F.P. and DeWitt, D.P., Fundamentals of heat and mass transfer, 3rd Ed., New York, John Wiley & Sons, (1990).
28. Abdel-Khalik, S.I., "Heat removal factor for a flat-plate solar collector with a serpentine tube", ***Solar Energy***, Vol. 18, No. 1, (1976), 59-64. (https://doi.org/10.1016/0038-092X(76)90036-0).
29. Hammami, M., Torretti, S., Grimaccia, F. and Grandi, G., "Thermal and performance analysis of a photovoltaic module with an integrated energy storage system", ***Applied Sciences***, Vol. 7, No. 11, (2017). (https://doi.org/10.3390/app7111107).
30. Santbergen, R., Rindt, C.C.M., Zondag, H.A. and Van Zolingen, R.J.Ch., "Detailed analysis of the energy yield of systems with covered sheet and tube PVT collectors", ***Solar Energy***, Vol. 84, No. 5, (2010). 867-878. (https://doi.org/10.1016/j.solener.2010.02.014).